Sensors and Materials, Vol. 38, No. 8 (2026) 5017–5030
MYU Tokyo

S & M 4608

Experimental Study on the Heave–Pitch Motions of a Rotating-buoy-type Wave Energy Converter

Jae-Seon Yoon,[1] Dongwoo Lee,[2] and Taemin Ha[3*]

[1]Korea Rural Community Corporation, Water Safety and Environmental Office Hydraulic Research Center, Ansan 15634, Korea
[2]Department of Civil & Construction Engineering, Kangwon National University, Samcheok 25913, Korea
[3]Department of Civil Engineering, Kangwon National University, Samcheok 25913, Korea

(Received December 15, 2025; accepted August 7, 2026)

Keywords: floating breakwater, hydraulic model experiment, response amplitude operator

Driven by the increasing need for coastal protection under climate change and the growing demand for renewable energy, integrated concepts that combine coastal protection with wave energy harvesting have attracted increasing attention. In this study, we propose a semi-cylindrical rotating-buoy-type wave energy converter installed at the front of a floating breakwater and experimentally investigated its dynamic response characteristics. Hydraulic model experiments were conducted under regular wave conditions. The buoy motions were quantified by video-based motion analysis, and the response amplitude operators for heave and pitch were determined. The results revealed a transition in the dominant motion mode with increasing wave period. Heave response is more pronounced in short-period waves, whereas pitch response becomes dominant under long-period wave conditions. These findings suggest that the design of floating bodies and moving-body-type wave energy converters should account for site-specific wave characteristics. Motion-oriented designs considering the dominant response mode may contribute to the more efficient optimization of wave energy conversion systems.

1. Introduction

The global community is facing the dual challenges of climate change and increasing energy demand, leading to a transition away from fossil-fuel-based energy systems toward more sustainable alternatives. Among marine renewable energy resources, ocean wave energy is often considered a reliable, high-potential, and attractive option. Its reliability is commonly attributed to the predictability and forecastability of wave conditions and the sustained propagation of wave energy over long distances, while its high power potential is associated with the high density of seawater compared with that of air.(1–3) Wave energy also exhibits high power intensity, typically reported to be on the order of 2–3 kW/m², which is substantially higher than those of solar energy (approximately 0.1–0.2 kW/m²) and wind energy (0.4–0.6 kW/m²).(4)

*Corresponding author: e-mail: tmha@kangwon.ac.kr
https://doi.org/10.18494/SAM6209

ISSN 0914-4935 © MYU K.K.
https://myukk.org/

Accordingly, a wide range of wave energy converters (WECs) has been developed to convert wave energy into electricity, including moving-body-type converters, oscillating water column (OWC) systems, and overtopping-type converters.

In coastal, harbor, and aquaculture environments, wave-control structures are essential for reducing incident wave forces and ensuring the safety of facilities and users. Conventional gravity-type breakwaters, such as caisson and rubble mound structures, have been widely adopted. However, they present several limitations, including rapidly increasing construction costs with water depth, the disruption of coastal circulation, and unintended shoreline changes such as erosion and sedimentation.(5,6) As an alternative, floating breakwaters (FBWs) composed of buoyant bodies and mooring systems have been proposed. These systems offer broader applicability across varying water depths and seabed conditions, and their modularity, ease of relocation, and potential for expansion make them increasingly useful for aquaculture farms, small harbors, and marine recreational areas.

At the same time, growing interest in decentralized marine renewable energy systems has highlighted the potential of multifunctional coastal structures, particularly in coastal and island regions where grid access is limited or where reliance on diesel generators remains prevalent. In this context, FBWs capable of simultaneously providing wave attenuation and power generation can serve as an effective alternative. By integrating a WEC into the floating structure or linking the motion of the breakwater to an energy conversion mechanism, a portion of the incident wave energy can be harvested for power production while concurrently enhancing wave-dissipation performance.

Numerous hybrid breakwater–WEC systems have been proposed for simultaneous coastal protection and renewable energy generation. Early developments in hybrid breakwater–WEC systems primarily focused on fixed breakwaters. Takahashi incorporated an OWC into a caisson breakwater,(7) whereas Margheritini *et al.* and Vicinanza *et al.* proposed overtopping-based WECs integrated with rubble-mound breakwaters.(8,9) In addition, Park *et al.* numerically evaluated the hydrodynamic performance of an OWC-based WEC applicable to breakwaters using computational fluid dynamics.(10) Peng *et al.* experimentally investigated the hydrodynamic performance of a hybrid system consisting of a fixed breakwater and multiple oscillating pontoons, evaluating both wave attenuation and wave energy conversion efficiency.(11)

More recently, research has expanded toward FBW-based hybrid systems. Ning *et al.* proposed a pile-restrained FBW operating as an oscillating-buoy-type WEC and experimentally evaluated its hydrodynamic performance.(12) Zhao *et al.* subsequently analyzed the hydrodynamic performance of an oscillating buoy WEC integrated into a pile-restrained FBW.(13) Zhang *et al.* analyzed the hydrodynamic performance of an FBW as an oscillating-buoy-type WEC and evaluated its wave attenuation and wave energy extraction performance.(14) Cheng *et al.* analyzed modular WEC-type FBWs arranged as an array at the fore-end of a very large floating structure and evaluated wave energy extraction and hydroelastic response reduction.(15) Wei *et al.* proposed a heave-hinge WEC combined with an FBW and numerically analyzed its wave attenuation and energy conversion performance.(16)

In this study, we aimed to experimentally investigate the dynamic response characteristics of an FBW equipped with a rotating-buoy-type WEC installed at the front of the FBW. The response characteristics were identified by analyzing the response amplitude operators (RAOs) for the heave and pitch motions of the buoy under regular wave conditions. Rather than focusing on power generation performance, we emphasized the kinematic and hydrodynamic responses of the rotating buoy, with the goal of providing fundamental data for the design and real-sea application of wave-energy-integrated FBW.

2. Methods

2.1 Wave control mechanism

The rotating-buoy-type WEC-FBW proposed in this study is based on a concept of stepwise control of incident wave energy by installing a rotating buoy with a vertical plate at the front of an FBW. First, incident waves induce heave and pitch motions in the rotating buoy system. The kinetic energy associated with these motions is transmitted to the generator shaft through a belt-driven power transmission mechanism, where it is converted into electrical energy. A large pulley ratio is applied between the driving pulley and the driven pulley so that a sufficient rotational speed can be achieved at the generator shaft even under relatively small buoy displacements and velocity variations.

Subsequently, the FBW body itself interacts with the remaining wave energy and induces additional reflection and dissipation effects. Through this process, the wave energy transmitted to the lee side of the structure is further reduced, allowing the system to simultaneously perform a wave attenuation function for coastal protection.

The rotating-buoy-type WEC consists of a semi-cylindrical buoy located near the free surface and a vertically oriented vertical plate attached beneath it. The semi-cylindrical buoy primarily induces vertical heave responses under incident wave action, while the vertical plate increases the moment about the rotational center and enhances the pitch response. Through the combined configuration of the upper semi-cylindrical buoy and the vertical plate, the rotating buoy is capable of simultaneously utilizing heave and pitch motion modes generated by incident waves. This configuration provides a mechanism that enhances both wave energy absorption and wave control performance at the front of the FBW (Fig. 1).

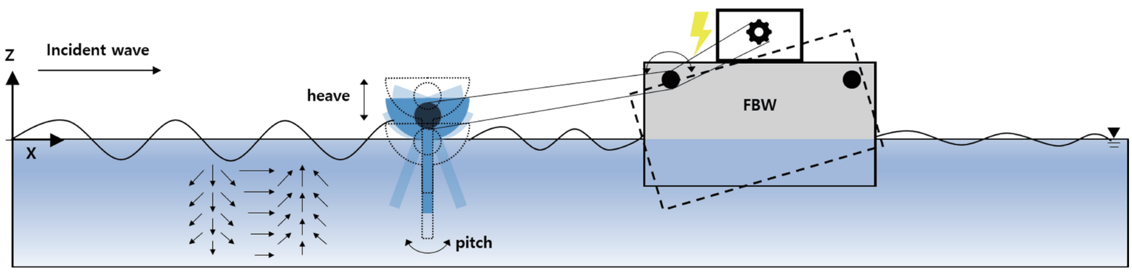

Fig. 1. (Color online) Rotating-buoy-type WEC-FBW mechanism.

2.2 Experimental facility

The hydraulic experiments in this study were conducted in an indoor wave flume located at the Rural Research Institute of the Korea Rural Community Corporation. The wave flume measures 66.0 m in length, 1.5 m in width, and 2.0 m in height. A 10-cm-thick vertical partition wall is installed at the center of the flume, dividing it into two separate channels: an observation channel and a calibration channel. The observation channel includes an approximately 18.0-m-long viewing window, which allows the real-time external monitoring of incident waves and the motion of the rotating buoy positioned in front of the FBW.

Wave generation was performed using a piston-type servo-motor wave maker in which the actuator drives the wave board through linear reciprocating motion. The wave board has dimensions of 1.5 m × 1.5 m, and its main specifications are summarized in Table 1.(17) The wave maker is capable of generating both regular and irregular waves on the basis of Bretschneider–Mitsuyasu and JONSWAP spectra, providing an experimental environment suitable for analyzing the dynamic behavior of the FBW and the rotating buoy under a wide range of wave conditions.

Wave absorbers are installed at both ends of the flume to effectively dissipate reflected waves during the experiments. Each absorber consists of an 8.0-m-long sloping beach with an inclination of approximately 12°, designed to reduce wave reflection and minimize the distortion of the wave field within the flume. This configuration ensures the stable propagation of waves generated by the wave maker and improves the accuracy of wave measurements and motion-response observations around the test structure.

2.3 Model of FBW

The hydraulic model used in this study was constructed as a model with a scale ratio of 1/30, following the Froude similarity law. The FBW model has overall dimensions of 0.60 m in length, 0.54 m in width, and 0.28 m in height. A rotating-buoy-type WEC with a vertical plate is attached to the front face of the FBW, forming an integrated configuration.

The rotating buoy with a vertical plate consists of a semi-cylindrical buoy located near the free surface and a vertical plate connected beneath it. The semi-cylindrical buoy has a diameter of 0.20 m, and a vertical plate with a length of 0.32 m in the vertical direction is installed below

Table 1
Specifications of the wave maker.

Category	Description	Remarks
Wave type	Regular and irregular waves	Bretschneider-Mitsuyasu JONSWAP
Wave board dimensions	1.5 m (B) × 1.5 m (H)	
Target (max) wave height	0.3 m (irregular waves) 0.5 m (regular waves)	
Max period	Up to 4.0 s	
Type	Piston type	
Driving mechanism	Electrical servo driven system	

the buoy with respect to the buoy's central rotational axis. A pulley is mounted at the top of the buoy, which serves not only as a component of the belt-driven power transmission mechanism but also as a reference geometry for video-based motion tracking. In addition, a yellow marker is attached to the surface of the vertical plate to enable the precise tracking of its motion, and this marker is used as a reference point for measuring the heave and pitch motions. The model was fabricated using acrylic material, and the overall configuration and components of the completed hydraulic model are shown in Fig. 2.

2.4 Measuring instruments

To verify the reproducibility of the target wave conditions and to quantitatively measure the characteristics of incident waves, three digital wave gauges were employed. The wave gauges were connected in series using a single cable, and the measured signals were converted into digital format for direct storage and processing on a computer. Each wave gauge has a maximum measurement range of 1.0 m, and the data sampling frequency was set to 20 Hz (0.05 s), which provides sufficient temporal resolution to capture waveform variations under regular wave conditions.

For the validation of the generated wave conditions and comparison of wave characteristics in front of the structure, the wave gauges were installed in both the observation channel and the calibration channel. In the observation channel, two digital wave gauges, WG1 and WG2, were installed in front of the FBW. A two-point method[18] was applied to separate incident and reflected waves and to identify the characteristics of the incident waves formed within the flume. In the calibration channel, a digital wave gauge, WG3, was installed to confirm that the waves generated by the wave maker reached the target wave height and period under conditions unaffected by the presence of the structure. This arrangement enabled the simultaneous verification of wave reproducibility and assessment of wave field variations around the FBW.

The heave and pitch motions of the rotating buoy with a vertical plate were measured using a high-resolution camera fixed outside the wave flume. The camera supports a maximum resolution of 4K (3840 × 2160 px) and a frame rate of 60 frames per second (60 fps), allowing

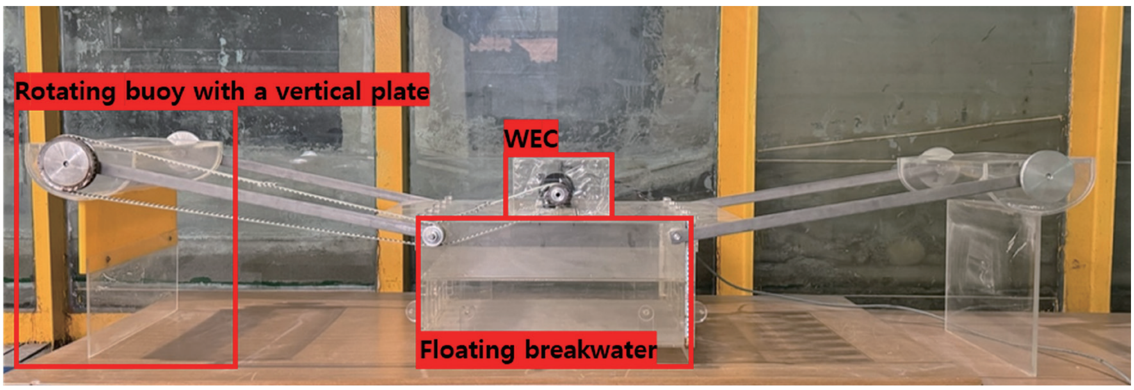

Fig. 2. (Color online) Model of rotating buoy with FBW.

relatively rapid buoy motions to be recorded without distortion. This setup provided stable and high-quality experimental images suitable for subsequent video-based analysis to evaluate the heave and pitch responses. The experimental equipment and its layout are shown in Fig. 3.

2.5 Experimental conditions

The experiments were conducted by generating unidirectional regular waves in the wave flume and measuring the heave and pitch motions of the rotating buoy with a vertical plate attached to the front of the FBW. The incident wave conditions were determined by considering the water depth of the flume, the wave-generation capability of the wave maker, and the relative relationship between the model scale and the incident wavelength. Wave heights and periods were combined to ensure the stable observation of the dynamic response characteristics of the buoy under each experimental condition. The applied regular wave conditions are summarized in Table 2.

The mooring system of the structure was configured using a taut-leg mooring arrangement. The experimental water depth was maintained at 0.60 m, and the taut-leg mooring was applied to suppress the horizontal motion of the FBW, thereby allowing the focused observation of the motion response characteristics of the rotating buoy with a vertical plate

3. Video-based RAO Evaluation

3.1 Coordinate tracking and RAO evaluation procedure

The motion of the rotating buoy was tracked using two reference points: the upper part of the pulley installed on the buoy and a marker attached to the vertical plate. The marker was mounted

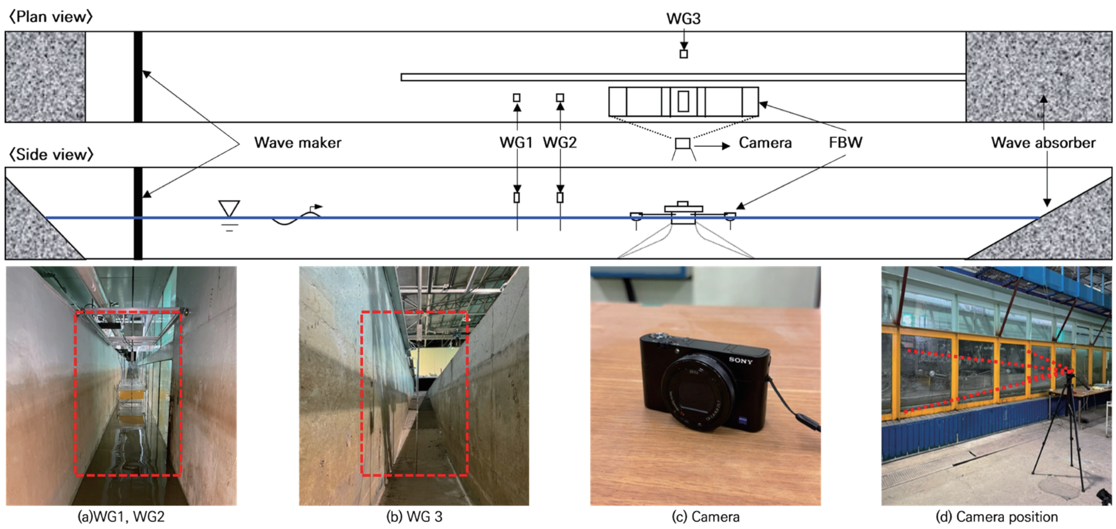

Fig. 3. (Color online) Experimental equipment and layout.

Table 2
Experimental conditions.

Depth 0.6 m	Wave height (m)	Wavelength (m)	Wave number	Wave period	Relative depth	Wave steepness
Case 1	0.12	2.27	2.77	1.25	0.26	0.05
Case 2	0.12	2.99	2.10	1.50	0.20	0.04
Case 3	0.12	3.69	1.70	1.75	0.16	0.03
Case 4	0.12	4.36	1.44	2.00	0.14	0.03
Case 5	0.12	5.03	1.25	2.25	0.12	0.02
Case 6	0.10	2.27	2.77	1.25	0.26	0.04
Case 7	0.10	2.99	2.10	1.50	0.20	0.03
Case 8	0.10	3.69	1.70	1.75	0.16	0.03
Case 9	0.10	4.36	1.44	2.00	0.14	0.02
Case 10	0.10	5.03	1.25	2.25	0.12	0.02
Case 11	0.08	2.27	2.77	1.25	0.26	0.04
Case 12	0.08	2.99	2.10	1.50	0.20	0.03
Case 13	0.08	3.69	1.70	1.75	0.16	0.02
Case 14	0.08	4.36	1.44	2.00	0.14	0.02
Case 15	0.08	5.03	1.25	2.25	0.12	0.02
Case 16	0.06	2.27	2.77	1.25	0.26	0.03
Case 17	0.06	2.99	2.10	1.50	0.20	0.02
Case 18	0.06	3.69	1.70	1.75	0.16	0.02
Case 19	0.06	4.36	1.44	2.00	0.14	0.01
Case 20	0.06	5.03	1.25	2.25	0.12	0.01

at the upper end of the extension line of the buoy's central rotational axis so that it could represent both the heave and pitch motions of the buoy. From the recorded images, the x and y coordinates of the marker were extracted on a frame-by-frame basis in real time.

The experimental videos were continuously recorded over the entire test duration using the fixed camera described in Sect. 2.4. The extracted coordinate data were processed through post-processing procedures to remove noise and were subsequently converted into the time series of motion responses. In cases where automatic tracking accuracy was temporarily degraded by light reflections or shadows, manual correction was applied to ensure reliable coordinate extraction.

The spatial scale of the coordinate system was calibrated on the basis of the measured physical height of the FBW model. Specifically, the pixel coordinates obtained from the images were mapped to the actual lengths of the structure, allowing the tracked x and y coordinates to be converted into real-space displacements. The resulting heave and pitch displacement time series were then used to evaluate the response amplitudes for each wave period, and RAOs were determined by normalizing the response amplitudes with the corresponding incident wave heights.

3.2 Heave RAO evaluation

To quantitatively evaluate the motion characteristics of the structure under different wave conditions, an RAO was employed. The RAO is a parameter that numerically represents the sensitivity of a structure's motion response to incident waves in the frequency domain and serves as a key metric for comparing structural responses under different wave periods.[19,20] The heave RAO is defined as the ratio of the amplitude of the vertical motion response of the structure to that of the corresponding incident wave under a given wave condition, and it can be expressed as

$$RAO_{heave} = \frac{\zeta_a}{\zeta_\omega}, \tag{1}$$

where ζ_a is the vertical motion amplitude of the buoy and ζ_ω is the amplitude of the incident wave.

To analyze the heave motion response quantitatively, the vertical displacement in the y direction obtained from video-based motion tracking was used. The measured data were derived from time-dependent coordinate variations, from which the vertical displacement time series was calculated for each condition.

3.3 Pitch RAO evaluation

To quantitatively analyze the response characteristics of pitch motion, coordinate variations of two reference points tracked through video analysis were used: the upper reference point located at the pulley installed on the buoy and the lower reference point located on the vertical plate. The measured data were obtained as time-dependent coordinate changes, from which motion displacements were derived and analyzed according to the incident wave height and period. The incident wave conditions applied for the pitch response analysis were identical to those used for the heave response analysis.

The pitch RAO is defined as the ratio of the amplitude of the rotational motion response of the structure to that of the corresponding incident wave under a given wave condition, and it can be expressed as

$$RAO_{pitch} = \frac{\zeta_k}{\zeta_\omega}, \tag{2}$$

where ζ_a is the rotational motion amplitude of the buoy and ζ_k is the amplitude of the incident wave.

The evaluation of pitch response requires a procedure to quantitatively determine the rotational motion of the structure, which cannot be accurately described using a single reference point. Since rotational motion occurs as a combination of vertical and horizontal movements about the central rotational axis, the pitch angle was calculated using the relative displacement between two reference points. Specifically, the upper reference point at the pulley and the lower reference point on the vertical plate were used to estimate the rotation angle of the buoy from their relative coordinate changes.

The rotation angle was determined from the slope of the vector formed by the two reference points, calculated using the positions obtained from consecutive frames in the time series. The positions of the reference points in the preceding frame (X_1, X_2) and the subsequent frame (Y_1, Y_2) were used to evaluate the temporal variation in rotation angle, and the conceptual procedure for this calculation is shown schematically in Fig. 4.

The rotation angle obtained from this procedure can be directly used for RAO analysis. However, to ensure consistency in comparative analysis with the heave response, the pitch response was converted into a length-based quantity and normalized into the same dimensionless form as the heave response. For this purpose, the pitch response was expressed as an arc length by multiplying the distance between the two reference points by the corresponding rotation angle, and the pitch RAO was calculated on the basis of this arc-length representation.

4. Results and Discussion

4.1 Heave response characteristics

The heave response generally exhibited higher values in the short-period range and showed a gradual decrease in amplitude as the wave period increased. In particular, the heave RAO reached its maximum under the wave period of 1.25 s, after which the response amplitude decreased beyond the period of 1.50 s. This period-dependent response trend was consistently observed at all wave heights.

Around the wave period of 1.75 s, the heave RAO exhibited its minimum, and the response amplitude gradually increased again with further increase in wave period. However, even in the long-period range of 2.00–2.25 s, the heave response did not reach the maximum level observed under short-period conditions and instead showed a relatively moderate recovery trend. These period-dependent variations in heave response are presented in Fig. 5 in the form of heave RAO curves for different wave heights.

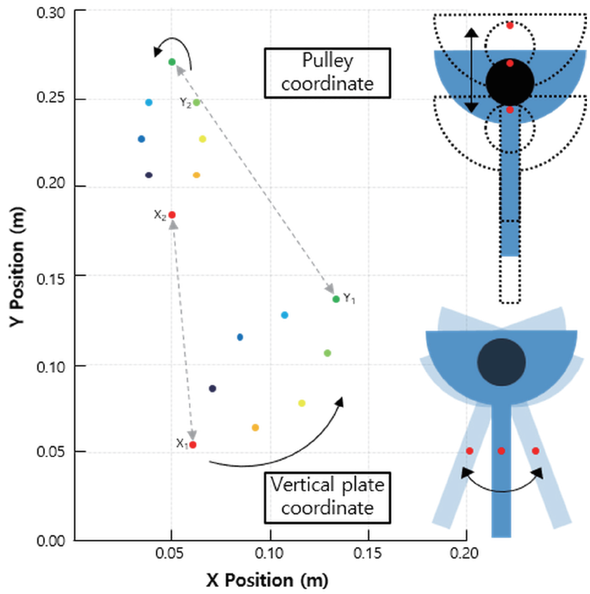

Fig. 4. (Color online) Pitch RAO.

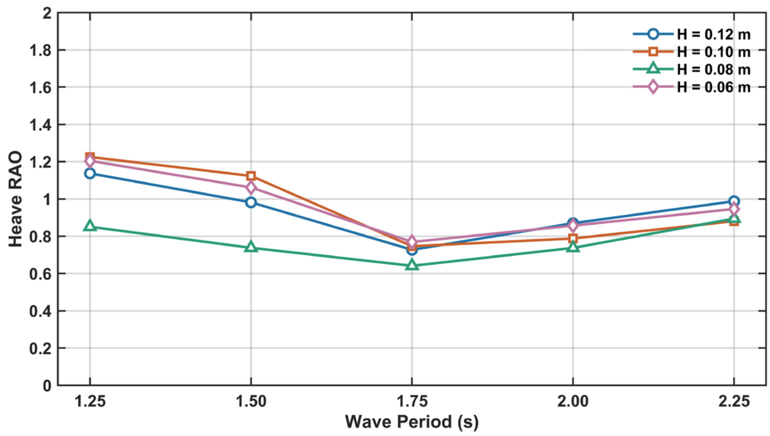

Fig. 5. (Color online) Variations in heave RAO with wave conditions.

The observed heave response characteristics are considered to be related to the structural configuration of the rotating buoy, which directly receives vertical wave-induced forces. In the short-period range, the repeated action of incident waves at short time intervals induces the relatively active vertical motion of the buoy. As the wave period increases, changes in the level of interaction between the wave action period and the structural response characteristics lead to a reduction in heave response.

4.2 Pitch response characteristics

In contrast, the pitch response generally exhibited an increasing trend with increasing wave period, and this characteristic became more pronounced in the long-period range. Under the wave period of 2.00 s, the pitch RAO reached its maximum at all wave heights, indicating that rotational motion was most dominant within the experimental range. The period-dependent variations in pitch RAO for different wave heights are presented in Fig. 6.

In the wave period range of 1.25–1.50 s, the pitch RAO remained relatively low. However, the response amplitude began to increase beyond the wave period of 1.75 s and reached its maximum at 2.00 s. At the wave period of 2.25 s, the pitch RAO showed a slight decrease or a relatively moderate variation, while remaining higher than the values observed in the short-period range. These period-dependent response trends were consistently observed across all wave heights, and the relative differences in pitch response due to wave height variations were found to be limited.

Notably, a transition region was observed beyond the wave period of 1.50 s, where the magnitudes of the heave RAO and pitch RAO became comparable. Beyond this region, the heave response gradually diminished, whereas the pitch response continued to increase. This transition demonstrates that the dominant motion mode of the structure shifts from vertical motion to rotational motion as the wave period increases, and quantitatively confirms that rotational motion becomes the primary dynamic response of the structure under long-period wave conditions.

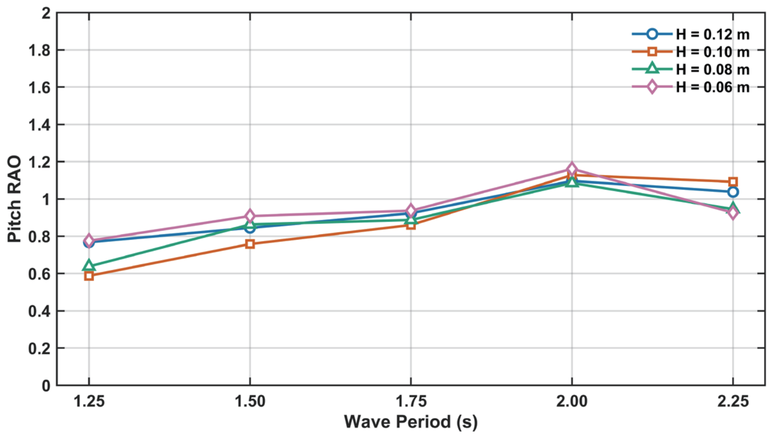

Fig. 6. (Color online) Variations in pitch RAO for different wave heights.

4.3 Ratio between heave and pitch responses

Figure 7 shows the variations in the relative contributions of the heave and pitch RAOs under different wave conditions. The results indicate that, in the short-period range of 1.25–1.50 s, the heave contribution is higher, suggesting that vertical motion acts as the dominant response mode of the buoy under short-period wave conditions. In this range, the incident waves act on the buoy at short time intervals, and although rotational motion occurs frequently, the associated angular displacement remains relatively small. As a result, the contribution of the pitch response is limited.

In contrast, in the longer-period range beyond approximately 1.75 s, the pitch response ratio gradually increases, indicating a transition in which rotational motion becomes the dominant dynamic response of the structure. Under long-period wave conditions, the increased wave period leads to larger angular displacements of the buoy, and consequently, the pitch response is progressively amplified. This response characteristic appears concurrently with the reduction in heave response and quantitatively demonstrates a transition in the wave energy transfer mechanism from vertical motion to rotational motion.

Such variations in heave-to-pitch response ratio indicate that the dominant motion mode of the rotating-buoy-type WEC depends strongly on the wave period. While vertical-motion-based energy absorption is more pronounced in the short-period range, rotational motion may serve as a more effective response mechanism under longer-period wave conditions.

4.4 Discussion

The experimental results show that the dynamic response of the rotating-buoy-type WEC integrated with the FBW is strongly governed by wave period, with a transition in the dominant motion mode. In the short-period range, the system response is characterized primarily by heave motion, whereas pitch motion becomes increasingly dominant as the wave period increases. This trend is consistently observed across all tested wave heights, indicating that the response

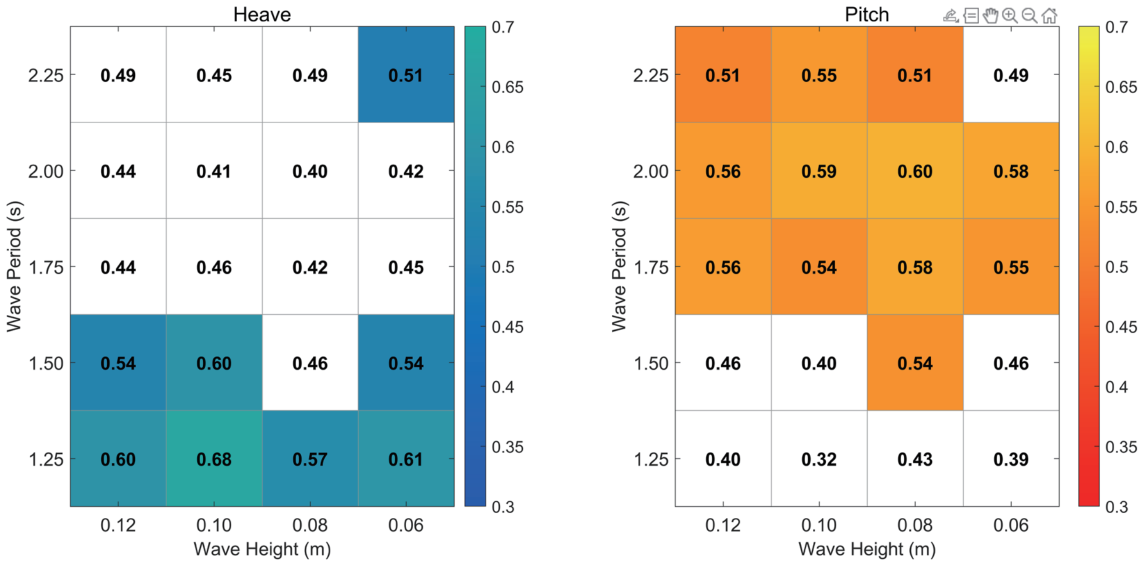

Fig. 7. (Color online) Ratio of heave RAO to pitch RAO.

characteristics within the present experimental range are more sensitive to wave period than to wave height.

The reduction in heave response with increasing wave period can be attributed to the direct vertical excitation mechanism acting on the buoy. Under short-period wave conditions, wave forces act on the buoy at short time intervals, leading to frequent vertical loading and relatively strong heave motion.

In contrast, the amplification of the pitch response under long-period wave conditions appears to be associated with the geometric configuration of the system, particularly the spacing between the FBW and the rotating buoy. In the setup, the FBW–buoy distance was approximately 1.0 m, which is comparable to one quarter of the incident wavelength at a wave period of 2.00 s (about 1.1 m). Under this condition, the buoy exhibited the largest pitching displacement within the tested range, suggesting that the spatial scale of the configuration is favorable for maximizing pitch motion when one wave cycle propagates across the FBW–buoy spacing.

Overall, the results indicate that the dominant motion mode of the rotating buoy differs depending on the target wave environment, with heave motion being more pronounced in short-period waves and pitch motion becoming dominant in long-period waves. This suggests that, when designing floating-body- or moving-body-type WECs, the dominant response mode should be identified on the basis of the wave characteristics of the deployment site. Designing the energy conversion mechanism to effectively utilize the dominant motion mode is expected to improve the overall energy conversion efficiency of integrated FBW–WEC systems.

5. Conclusions

In this study, we experimentally investigated the dynamic response characteristics of a rotating-buoy-type WEC integrated with an FBW under regular wave conditions. Hydraulic model tests were conducted using a 1/30-scale model, and the motion responses were quantified through video-based motion tracking and RAO analysis.

The results showed that the heave response was dominant in the short-period wave range, while the pitch response became increasingly significant as the wave period increased. A clear transition in the dominant motion mode from heave to pitch was observed around a wave period of 1.50–1.75 s, indicating that wave period plays a critical role in governing the dynamic behavior of the integrated system.

The maximum pitch response occurred at a wave period of 2.00 s, which is considered to be associated with the geometric relationship between the spacing of the rotating buoy and the FBW and the incident wavelength. When the buoy–breakwater spacing became comparable to approximately one quarter of the incident wavelength, a favorable spatial phase relationship was formed, leading to the enhanced rotational motion of the buoy. These findings indicate that the dominant response mode of the rotating-buoy-type WEC depends strongly on the target wave environment. While vertical motion is more effective in short-period waves, rotational motion becomes more advantageous under long-period wave conditions. Therefore, the design of floating-body- or moving-body-type WECs should account for site-specific wave characteristics and prioritize the utilization of the dominant motion mode to improve overall energy conversion efficiency.

The study provides fundamental experimental insights into the motion behavior of integrated FBW–WEC systems and offers useful guidance for the motion-oriented design and optimization of WECs for practical marine applications.

Acknowledgments

This study was funded by the Basic Science Research Program through the National Research Foundation of Korea (NRF), funded by the Ministry of Science and ICT, South Korea (RS-2023-00209256, RS-2022-00144263).

References

1 A. S. Bahaj: Renew. Sustain. Energy Rev. **15** (2011) 3399. https://doi.org/10.1016/j.rser.2011.04.032
2 J. F Chozas: Technical and Non-Technical Issues Towards the Commercialization of Wave Energy Converters. Ph.D. dissertation, Aalborg University (2013).
3 J. Cruz: Ocean Wave Energy: Current Status and Future Perspectives (Springer, Berlin 2008).
4 B. Drew, A. R. Plummer, and M. Sahinkaya: Proc. Inst. Mech. Eng. A J. Power Energy **223** (2009) 887. https://doi.org/10.1243/09576509JPE782
5 C. Y. Ji, X. Chen, J. Cui, Z. M. Yuan, and A. Incecik: Ocean Eng. **105** (2015) 295. https://doi.org/10.1016/j.oceaneng.2015.06.046
6 J. Dai, C. M Wang, T. Utsunomiya, and W. Duan: Ocean Eng. **158** (2018) 132. https://doi.org/10.1016/j.oceaneng.2018.03.083
7 S. Takahashi, S. (1988). Proc. 21st Int. Conf. Coastal Engineering (ASCE, 1989) 2489. https://doi.org/10.1061/9780872626874.186
8 L. Margheritini, D. Vicinanza, and P. Frigaard: Renew. Energy **34** (2009) 1371. https://doi.org/10.1016/j.renene.2008.10.005
9 D. Vicinanza, P. Contestabile, J. Q. H. Nørgaard, and T. L. Andersen: Coastal Eng. **88** (2014) 154. https://doi.org/10.1016/j.coastaleng.2014.02.004

10 S. Park, K. H. Kim, B. W. Nam, J. S Kim, and K. Hong: J. Korean Soc. Mar. Environ. Energy **21** (2018) 317. https://doi.org/10.7846/JKOSMEE.2018.21.4.317

11 W. Peng, Y. Zhang, X. Yang, J. Zhang, R. He, Y. Liu, and R. Chen: Energies **13** (2020) 5740. https://doi.org/10.3390/en13215740

12 D. Ning, X. Zhao, M. Göteman, and H. Kang: Renew. Energy **95** (2016) 531. https://doi.org/10.1016/j.renene.2016.04.057

13 X. Zhao, D. Ning, C. Zhang, and H. Kang: Energies **10** (2017) 712. https://doi.org/10.3390/en10050712

14 H. Zhang, B. Zhou, C. Vogel, R. Willden, J. Zang, and L. Zhang: Appl. Energy **257** (2020) 113996. https://doi.org/10.1016/j.apenergy.2019.113996

15 Y. Cheng, C. Xi, S. Dai, C. Ji, M. Collu, M. Li, Z. M. Yuan, and A. Incecik: Appl. Energy **306** (2022) 117953. https://doi.org/10.1016/j.apenergy.2021.117953

16 Y. Wei, S. Yu, X. Li, C. Zhang, D. Ning, and L. Huang: Ocean Eng. **293** (2024) 116618. https://doi.org/10.1016/j.oceaneng.2023.116618

17 J. S. Yoon, B. W. Lee, D. Ko, U. J. Lee, D. Lee, and T. Ha: J. Coast. Res. Special Issue **116** (2023) 66. https://doi.org/10.2112/JCR-SI116-014.1

18 Y. Goda and Y. Suzuki: Proc. 15th Int. Conf. Coastal Engineering (ASCE, 1976) 828. https://doi.org/10.1061/9780872620834.048

19 J. N. Newman: Marine Hydrodynamics (MIT Press, Cambridge, MA, 1977).

20 O. M. Faltinsen: Sea Loads on Ships and Offshore Structures (Cambridge University Press, Cambridge, 1993).